

EUV Interferometry of the 0.3 NA MET Optic

Kenneth A. Goldberg^{*a}, Patrick Naulleau^a, Paul Denham^a, Senajith B. Rekawa^a, Keith Jackson^a,
Erik H. Anderson^a, J. Alexander Liddle^a, Jeffrey Bokor^{a,b}

^aCenter for X-Ray Optics, Lawrence Berkeley National Laboratory, Berkeley, CA 94720

^bECS Department, University of California, Berkeley, CA 94720

ABSTRACT

A new generation of 0.3 numerical aperture prototype EUV optical systems is now being produced to provide an opportunity for early learning at 20-nm feature size. Achieving diffraction limited performance from these two-mirror, annular projection optics poses a challenge for every aspect of the fabrication process, including final alignment and interferometric qualification. A new phase-shifting point diffraction interferometer will be used at Lawrence Berkeley National Laboratory for the measurement and alignment of the MET optic at EUV wavelengths. Using the previous generation of prototype EUV optical systems developed for lithography research, with numerical apertures up to 0.1, EUV interferometers have demonstrated RMS accuracy levels in the 40–70 pm range. Relative to the previous generation of prototype EUV optics, the threefold increase to 0.3 NA in the image-side numerical aperture presents several challenges for the extension of ultra-high-accuracy.

Keywords: interferometry, extreme ultraviolet lithography, EUV, at-wavelength testing, MET.

1. INTRODUCTION

High-accuracy interferometry is a cornerstone requirement for the success of EUV optical systems. State-of-the-art visible-light testing is used in the fabrication of the individual mirror elements,^{1,2} and has been used in the alignment of numerous assembled EUV optical systems.^{3,4,5} Interferometer absolute accuracies in the 50 pm range are a requirement for the measurement of production-quality EUV elements and assembled systems.⁶

Visible-light interferometry continues to benefit by close, ongoing comparisons with EUV interferometric measurements performed on the same optical systems. A system-level comparison performed at more than 40 points across the field of view of the Engineering Test Stand (ETS) Set-2 optic, revealed a level of agreement of 0.35 ± 0.11 nm between EUV and visible light interferometries.⁷ The discrepancy was concentrated in the lowest spatial frequency aberrations (astigmatism in particular) which are most important for the alignment of the system. Recently, several systematic measurement error sources have been identified via comparison, and subsequently addressed. This continuing learning raises the accuracy of the visible-light interferometric techniques.

EUV interferometry performed with the phase-shifting point diffraction interferometer (PS/PDI)^{8,9} has demonstrated accuracy levels of 40-70 pm during the testing of previous generations of prototype EUV optical systems, typically of 0.1 NA, developed for EUV lithography research.¹⁰

Often, prior to measurements with the PS/PDI, the optics are measured with lateral shearing interferometry (LSI) which is performed with a cross-grating transmission beamsplitter placed near the image-plane.¹¹ As reported previously, for the initial measurement of a nominally pre-aligned test optic, the LSI has several advantages over the PS/PDI. These include ease of alignment, high efficiency, and the potential to measure aberrations of larger magnitudes. Switching between the PS/PDI and the LSI requires only a change of the image-plane mask. (Since the experimental chamber is also designed for small-field imaging experiments¹², there is a built-in load-lock and manual wafer (or pinhole-mask) transfer system.)

Measurements performed at the operational EUV wavelengths, at-wavelength, remove potential uncertainties about the response of the resonant-reflective multilayer coatings, and have provided accurate predictions of imaging

*Correspondence: Email: KAGoldberg@lbl.gov; Telephone: 510-495-2261; Fax: 510-486-4550

performance.^{13,14} Relative to visible-light interferometry, the considerably shorter EUV wavelength reduces the length scale of reference and simplifies many aspects of interferometric measurement. EUV interferometry has been used in the diagnosis and remediation of several types of fabrication and system-alignment errors, in the assessment of chromatic effects¹⁵ and flare,¹⁶ and most importantly, in the optimization of imaging performance.

To date, seven EUV optics with numerical apertures between 0.08 and 0.1 have been tested and aligned. We report the development of at-wavelength testing of a two-mirror, annular, 0.3 NA *Micro Exposure Tool* (MET) optic,¹⁷ shown in Fig. 1. The interferometer is being built into the same experimental chamber as a small-field lithographic imaging system that will be used following interferometry and alignment.

There are several areas where the extension of interferometry to 0.3 NA poses significant challenges. Perhaps the foremost challenge is the fabrication and use of appropriately sized pinhole spatial filters, which are responsible for producing the nearly perfect spherical reference waves in the object (mask) and image (wafer) planes. The testing geometry also necessitates appropriate calibration of the interferometer to remove systematic aberrations.

2. MECHANICAL DESIGN

The interferometer is being built on an undulator beamline at the Advanced Light Source (ALS) synchrotron radiation facility at Lawrence Berkeley National Laboratory (LBNL). The beamline is optimized for high coherent flux near 13-nm wavelength, and has been used for all previous interferometry of reflective EUV optical systems performed by our group.^{18,19} The beamline incorporates a variable-line-space plane-grating monochromator and vertical exit slit which allows a tunable energy bandwidth $E/\Delta E$ of between 55 and 1300. An adjustable Kirkpatrick-Baez (K-B) mirror pair focuses the synchrotron beam into the object plane of the test optic with a numerical aperture of approximately 0.006 NA.²⁰

The new interferometer follows the design of previously reported PS/PDIs^{21,22} with components scaled or modified to accommodate the MET optical system. The interferometer is designed to perform wavefront measurements at multiple points across the field of view of the optical system, and in the longitudinal direction. Intended for use with reflective masks, the design field of view spans a tilted plane with lateral dimensions of $200 \times 600 \mu\text{m}$, at a 0.8° angle in the image plane. The conjugate object field is $1000 \times 3000 \mu\text{m}$, at 4.0° tilt in the Scheimpflug imaging condition. The longitudinal range of the interferometer's stages is 2 mm, enabling measurements across arbitrary planes of interest within the three-dimensional field of view.

Excluding the beamline, the optical components of the interferometer are the object- and image-plane pinhole masks, a coarse transmission grating beam-splitter, and an EUV CCD camera. Light enters the MET vertically from above: the illuminating beam is aligned to be coincident with the optic axis. Figure 2 is a mechanical drawing showing how the MET is supported within the vacuum chamber.

2.1 Object stage

A high-resolution translation stage holds the pinhole mask in the object plane. The stage has five degrees of freedom which include x , y , z , θ_x , and θ_y . The mask contains a variety of *object pinhole* sizes and slightly larger alignment marks arranged into groups, one for each of 9 points in the field of view. These 9 points form a 3×3 grid spanning the $1000 \times 3000\text{-}\mu\text{m}$ field in the object plane. All of the mask features are open stencil, passing through the nickel absorber and the silicon-nitride membrane that supports them. The pinhole sizes appropriate for the 0.06 input NA of the MET are between 100 and 200-nm diameter. A pinhole-to-pinhole separation greater than $50 \mu\text{m}$ ensures that only one object pinhole is illuminated at a time. Owing to the small size of the MET's field of view, the pinhole mask is fabricated in a single membrane.



Figure 1: Photo of the MET optical system resting on a stand. Photo courtesy of John Taylor, LLNL.

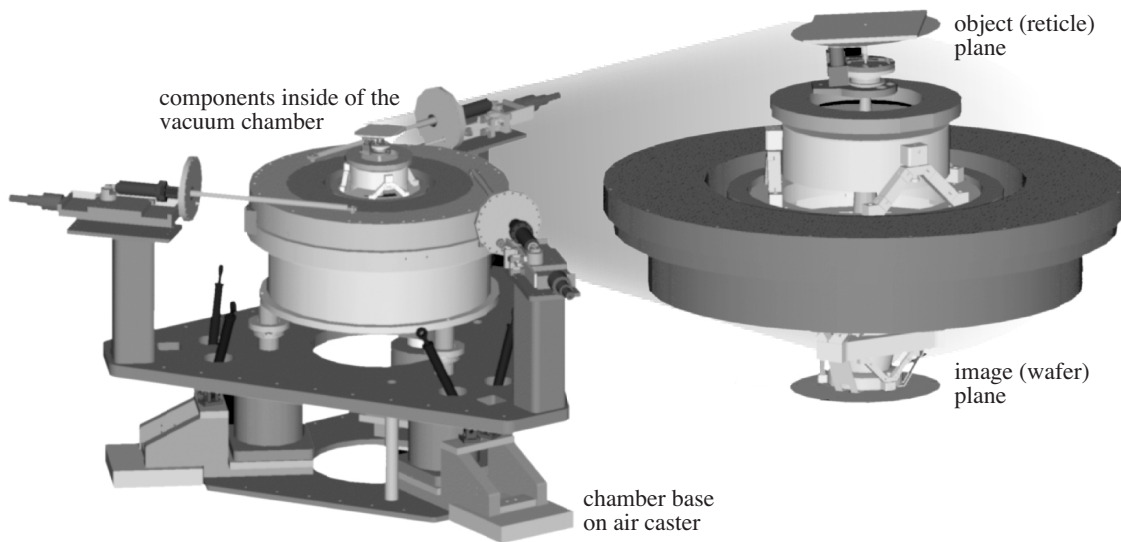


Figure 2: Mechanical drawing of the interior components of the experimental test chamber configured for MET measurement. At right is an expanded view of the MET as it is held in an annular support ring. Object and image-plane components are shown schematically.

2.2 Grating stage

Below the object plane, a multi-purpose retractable stage holds a transmission grating beamsplitter, and a single-element photodiode for flux monitoring and to assist in aligning the illuminating beam through the object pinholes. The longitudinal position of the grating, which affects the separation distance of the test and reference beams in the image plane, can be adjusted with the whole arm mechanism. The grating has additional degrees of freedom that are used for phase-shifting capability and for alignment—both the fine translational position of the grating and the rotation angle are controlled on a nested sub-stage.

2.3 Image stage

Below the optic, a similar high resolution five-degree of freedom stage holds the *image pinhole* mask in the image-plane. Open stencil mask window and pinhole features are grouped by field point. At each field point, there is an array of mask features, including pinholes of different sizes, so that the optimal size may be selected *in situ*. The required image-plane pinhole sizes are expected to be between 25 and 40-nm diameter.

2.4 Support structures

The object and image stages are rigidly supported by the same structure that supports the MET optic. These components move together on a planar-bearing stage coupled to the ground through a passive vibration-isolation system. To move from point to point within the field of view, the optic and the stages are translated together under the stationary illuminating beam. The grating stage, described above, is supported separately and does not move with the optic.

2.5 CCD detector

Below the MET, a back-thinned, back-illuminated EUV CCD camera with one-square inch area faces upward and records the transmitted light. The CCD camera has 1024×1024 square pixels. The camera is stationary; in order to capture the full pupil and accommodate the translation of the test optic, the detector plane of the CCD is positioned one inch (2.54 cm) below the image plane. The CCD chip is thermoelectrically cooled to approximately -35°C .

2.6 Conjugate point metrology tower

Since the aberrations of the optical system are field dependent, the accurate measurement and transfer of the conjugate point locations is critical to both the alignment process and to the inter-comparison of wavefront measurements performed on different interferometers (EUV interferometry at LBNL, and visible-light interferometry at LLNL). To enable measurement of the conjugate positions, a metrology tower has been constructed for the interferometer at LBNL. The metrology tower mounts kinematically to the support ring of the MET housing, and it provides a means for identifying the

central point in the object-side field of view, in three dimensions. Three upward-facing capacitance micrometers on the metrology tower measure the longitudinal position and tilt of the object-plane pinhole mask. The capacitance micrometers are separated by approximately 75 mm from each other. Two small, in-vacuum cameras fitted with microscope objectives measure the lateral positions of alignment features patterned on the mask.²³ To achieve a relative wavefront accuracy of 50 pm or below between the visible-light and the EUV interferometry, the field positioning tolerance is 125 μm laterally and 8 μm longitudinally. These specifications are within the capabilities of the sensors incorporated into the metrology tower. Ideally, a single metrology tower would be used for both the visible-light and EUV measurements. However, due to mechanical constraints, this proved infeasible, and a separate metrology tower will be used in the LLNL visible-light interferometer. A coordinate measuring machine serving as a fixed reference will be used to correlate sensor readings from the two towers.

2.7 Environment

EUV illumination of the MET will take place within a temperature-controlled vacuum chamber environment built to UHV standards. All components and materials are fabricated according to standards set for the Engineering Test Stand. We expect the chamber base pressures to be below 10^{-6} Torr. Similar to the interferometry performed on the ETS, the beamline endstation will be enclosed in an insulated, thermally controlled environment. Within the vacuum chamber the thermal time constants are very long; experience in testing ETS projection optics has shown that temperature stability of 0.01°C within an 8 hour period is achievable.

3. PINHOLE DEVELOPMENT AND TESTING

The accuracy of the PS/PDI interferometer relies on the quality of the spherical reference waves diffracted by small pinholes. In order to diffract a spherical wave covering the numerical aperture of measurement, the pinhole sizes are chosen equal to or smaller than the diffraction-limited resolution of the test optic. Furthermore, since the pinhole shape can influence the diffracted reference waves, the pinholes should be close to circular in cross-section. While the quality of the diffracted wavefronts generally improves with decreasing pinhole size, the accompanying reduction in transmitted power necessitates a compromise between pinhole size and wavefront quality.²⁴ The pinholes spatially filter the aberrated test beam, and as such, the quality of the reference wavefronts generally improves with the wavefront quality of the optic under test.

The pinholes used in the PS/PDI are fabricated with electron-beam lithography using LBNL's *Nanowriter*²⁵ tool. Nickel or gold membranes are used as the absorber layers in which the open-stencil pinholes are fabricated. For 0.1 NA optical system testing, the absorber membranes have been electroplated onto 100-nm-thick silicon-nitride membranes. In some cases, the absorber layers were deposited onto both sides of the membrane. Future pinhole masks may be made with the nitride-membrane removed with a dry-etch process.

Experience has shown that for testing 0.1 NA optics, the optimal pinhole sizes are in the 80–120-nm range. Extrapolating to 0.3 NA, the optimal pinhole sizes may be in the 30–40-nm range. For 80-nm pinholes, where the pinhole size is several EUV wavelengths in diameter, simple, thin-screen diffraction theory seems to predict the observed behavior well. However, for pinholes with diameters that are only 2 or 3 EUV wavelengths wide, and with much higher aspect ratios (thickness to diameter), the simple theory may be inadequate.

In preparation for the MET measurement, we are conducting research to fabricate and test and to model the behavior of these pinholes. Densely spaced arrays of nominally identical pinholes are fabricated in the Nanowriter and diffraction measurements are made on ALS beamline 6.3.2. A detail of one pinhole array is shown in Fig. 3. While the array produces a two-dimensional pattern of narrow peaks, the intensity envelope function of the collective diffraction pattern reveals the single-pinhole diffraction pattern. Through this ongoing research, we hope to establish the fabrication specifications of appropriate interferometry pinholes for a variety of NA values, and to improve the agreement between detailed pinhole-diffraction modeling and experimental data.

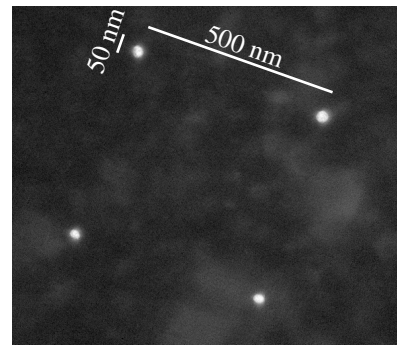


Figure 3: TEM micrograph of four sub-50-nm pinholes from within a dense pinhole array. Arrays of pinholes have been created during the development phase to measure the diffraction properties in aggregate.

4. GEOMETRIC CONSIDERATIONS

Unlike many conventional interferometers, the PS/PDI and LSI employed for the at-wavelength testing have no optical elements between the image-plane and the CCD detector. The predictable geometric path length difference between the test and the reference beams, propagating to the detector plane from displaced positions in the image-plane, accounts for a compensable systematic measurement error in the interferometer.²⁴

The magnitude of the geometric aberration terms, which are dominated by coma, is on the order of 3 nm RMS. There is an additional sensitivity of the measured astigmatism to the tilt of the detector plane of approximately 0.6 nm RMS per degree of tilt.

To measure and accurately compensate these systematic aberrations, our testing procedure includes the rotation of the image-plane beam-separation direction. The rotation is achieved by in-plane variation of the orientation of the beam-splitter grating, and using image-plane mask pinholes with different orientations. Since the magnitudes of the systematic aberrations are typically proportional to the beam-separation vector, this rotation can be used to isolate the aberration terms from the wavefront under test.

Separate from the aberrations that arise from the beam-separation, the projection of the spherical pupil wavefront onto a planar detector results in a radial distortion that must be compensated in the wavefront measurement. In previous measurements of EUV optical systems with NA values of 0.1 and below, the radial distortion magnitudes were limited to a fraction of a detector pixel. At 0.3 NA, with 600 pixels in the diameter of the measurement domain, the peak distortion will be approximately 3 pixels.²⁴

5. SUMMARY

Preparations for the EUV interferometric testing of the MET projection optic on undulator beamline 12.0.1 of the Advanced Light Source at Lawrence Berkeley National Laboratory are now underway. The interferometer will be housed in the same experimental chamber used to measure two sets of ETS projection optical systems. The chamber's interior has been modified to accommodate the smaller size and higher (0.3) numerical aperture of the MET.

The extension of phase-shifting point diffraction interferometry (PS/PDI) and lateral shearing interferometry (LSI) to 0.3 NA presents significant technical challenges. The fabrication of appropriately sized pinholes brings LBNL's Nanowriter e-beam lithography tool close to its current resolution limit. Furthermore, the compensation of geometric systematic aberrations in the wavefront analysis will require careful subtraction of much larger error terms than have been faced in the past. Using these same techniques, our group has demonstrated EUV interferometry accuracy levels of $\lambda_{\text{EUV}}/330$ RMS (41 pm) for 0.08 NA measurements,¹⁰ and below $\lambda_{\text{EUV}}/200$ RMS (67 pm) for 0.1 NA. The measurement and alignment of the MET optic will prepare it for EUV image-printing experiments at 20 nm feature size, and provide an opportunity to evaluate the accuracy and feasibility of EUV testing of relevant lithographic quality EUV optical systems.

This work is funded by the International Sematech, the EUV Limited Liability Corporation (LLC), and by the U.S. Department of Energy.

REFERENCES

1. G. E. Sommargren, "Phase shifting diffraction interferometer," U.S. Patent 5,548,403, August 20, 1996.
2. H. N. Chapman and D. W. Sweeney, "A rigorous method for compensation selection and alignment of microlithographic optical systems," *Proc. SPIE* **3331**, 102–13 (1998).
3. K. A. Goldberg, P. Naulleau, S. H. Lee, C. Chang, *et al.*, "Direct comparison of EUV and visible-light interferometries," *Proc. SPIE* **3676**, 635–42 (1999).
4. D. A. Tichenor, G. D. Kubiak, W. C. Replogle, L. E. Klebanoff, *et al.*, "EUV Engineering Test Stand," *Proc. SPIE* **3997**, 48–69 (2000).
5. K. A. Goldberg, P. Naulleau, J. Bokor, and H. N. Chapman, "Honing the accuracy of extreme ultraviolet optical system testing: at-wavelength and visible-light measurements of the ETS Set-2 projection optic," *Proc. SPIE* **4688**, 329–37 (2002).

6. D. W. Sweeney, "Status of EUVL enabling technologies," *these proceedings*.
7. K. Goldberg, P. Naulleau, J. Bokor and H. Chapman, "Testing EUV Optics with Visible-Light and EUV Interferometry," *J. Vac. Sci. & Technol. B* **20** (6), 2834–39 (2002).
8. H. Medeck, "Phase-shifting point diffraction interferometer," U.S. Patent No. 5,835,217, November 10, 1998.
9. H. Medeck, E. Tejnil, K. A. Goldberg, and J. Bokor, "A Phase-Shifting Point Diffraction Interferometer," *Opt. Lett.* **21** (19), 1526–8 (1996).
10. P. P. Naulleau, K. A. Goldberg, S. H. Lee, C. Chang, D. Attwood, and J. Bokor, "Extreme-ultraviolet phase-shifting point-diffraction interferometer: a wave-front metrology tool with subangstrom reference-wave accuracy," *Appl. Opt.* **38** (35), 7252–63 (1999).
11. P. P. Naulleau, K. A. Goldberg and J. Bokor, "Extreme ultraviolet carrier-frequency shearing Interferometry of a lithographic four-mirror optical system," *J. Vac. Sci. & Technol. B* **18** (6), 2939–43 (2000).
12. P. P. Naulleau, K. A. Goldberg, E. H. Anderson, J. Bokor, *et al.*, "Static EUV microexposures using the ETS set-2 optics," *these proceedings*.
13. P. Naulleau, K. A. Goldberg, E. Anderson, D. Attwood, *et al.*, "Sub-70-nm EUV Lithography at the Advanced Light Source Static Microfield Exposure Station Using the ETS Set-2 Optic," *J. Vac. Sci. & Technol. B* **20** (6), 2829–33 (2002).
14. E. Tejnil, K. A. Goldberg, S. H. Lee, H. Medeck, *et al.*, "At-wavelength interferometry for EUV lithography," *J. Vac. Sci. & Technol. B* **15** (6), 2455–61 (1997).
15. E. Tejnil, K. A. Goldberg, J. Bokor, "Phase effects owing to multilayer coatings in a two-mirror extreme-ultraviolet Schwarzschild objective," *Appl. Opt.* **37** (34), 8021–9 (1998).
16. P. Naulleau, K. A. Goldberg, E. M. Gullikson, and J. Bokor, "Interferometric at-wavelength flare characterization of EUV optical systems," *J. Vac. Sci. & Technol. B* **17** (6), 2987–91 (1999).
17. R. Hudyma, "High numerical aperture microstepper final optical design report," LLNL Internal Report M199900286, September 24, 1999.
18. D. T. Attwood, P. Naulleau, K. A. Goldberg, E. Tejnil, *et al.*, "Tunable coherent radiation in the soft x-ray and extreme ultraviolet spectral regions," *IEEE Journal of Quantum Electronics* **35** (5), 709–20 (1999).
19. R. Beguiristain, J. H. Underwood, M. Koike, P. Batson, *et al.*, "Characterization of thermal distortion effects on beamline optics for EUV interferometry and soft x-ray microscopy," *Rev. Sci. Instrumen.* **67** (9), 1–9 (1996).
20. P. P. Naulleau, K. A. Goldberg, P. J. Batson, S. Jeong, and J. H. Underwood, "Tolerancing of diffraction-limited Kirkpatrick-Baez synchrotron beamline optics for extreme-ultraviolet metrology," *Appl. Opt.* **40** (22), 3703–3709 (2001).
21. K. A. Goldberg, E. Tejnil, S. H. Lee, H. Medeck, *et al.*, "Characterization of an EUV Schwarzschild objective using phase-shifting point diffraction interferometry," *Proc. SPIE* **3048**, 264–70 (1997).
22. K. A. Goldberg, P. Naulleau, P. Batson, P. Denham, H. Chapman, and J. Bokor, "Extreme ultraviolet alignment and testing of a four mirror aspheric extreme ultraviolet optical system," *J. Vac. Sci. & Technol. B* **18** (6), 2911–15 (2000).
23. "Miniature self-contained vacuum compatible electronic imaging microscope," P. P. Naulleau, P. J. Batson, P. E. Denham, and M. S. Jones, U.S. Patent No. 6,327,102, March 7, 2000.
24. K. A. Goldberg, "Extreme Ultraviolet Interferometry," Ph.D. dissertation, Physics Department, University of California, Berkeley, 1997.
25. E. H. Anderson, D. Olynick, B. Harteneck, E. Veklerov, *et al.*, "Nanofabrication and Diffractive Optics For High-Resolution X-Ray Applications," *J. Vac. Sci. & Technol. B* **18** (6), 2970 (2000).